ANNUAL REVIEWS

Annual Review of Fluid Mechanics

Aeroacoustics of Silent Owl Flight

Justin W. Jaworski[1] and N. Peake[2]

[1]Department of Mechanical Engineering and Mechanics, Lehigh University, Bethlehem, Pennsylvania 18015, USA; email: jaworski@lehigh.edu

[2]Department of Applied Mathematics and Theoretical Physics, University of Cambridge, Cambridge CB3 0WA, United Kingdom; email: n.peake@damtp.cam.ac.uk

Annu. Rev. Fluid Mech. 2020. 52:395–420

First published as a Review in Advance on August 28, 2019

The *Annual Review of Fluid Mechanics* is online at fluid.annualreviews.org

https://doi.org/10.1146/annurev-fluid-010518-040436

Keywords

aeroacoustics, silent flight, noise generation, owl morphology

Abstract

The ability of some species of owl to fly in effective silence is unique among birds and provides a distinct hunting advantage, but it remains a mystery as to exactly what aspects of the owl and its flight are responsible for this dramatic noise reduction. Crucially, this mystery extends to how the flow physics may be leveraged to generate noise-reduction strategies for wider technological application. We review current knowledge of aerodynamic noise from owls, ranging from live owl noise measurements to mathematical modeling and experiments focused on how owls may disrupt the standard routes of noise generation. Specialized adaptations and foraging strategies are not uniform across all owl species: Some species may not have need for silent flight, or their evolutionary adaptations may not be effective for useful noise reduction for certain species. This hypothesis is examined using mathematical models and borne out where possible by noise measurements and morphological observations of owl feathers and wings.

1. INTRODUCTION

All solid bodies produce noise as a consequence of their motion through a fluid, often associated with the turbulent flow they produce and its interaction with the body. For many aerospace applications, noise production can be a major source of public annoyance and is often subject to regulatory barriers. For instance, at London Heathrow fines are levied on airlines that breach prescribed noise levels, with the nighttime limits some seven decibels lower than those during the day, i.e., more than halving the maximum allowed acoustic energy (CAA 2018). Continued public pressure is leading to yet more restrictive regulations and targets imposed on industry (High Level Group Aviat. Res. 2011, FAA 2019) at the same time that emission and performance standards (e.g., range, fuel efficiency, power off-take) must be improved, driving the need for highly innovative research and development (e.g., Hileman et al. 2007). One area of particular concern is airframe noise (due to, for instance, the interaction between turbulent flow and deployed wing devices and landing gear), which on conventional aircraft on approach can contribute as much to the noise signature as the engines (Crighton 1991). Such turbulence–structure interaction noise may also establish a regulatory barrier to alternative energy and emerging commercial transport, such as wind turbines (Oerlemans et al. 2007), electric air taxis (Seeley 2015), and small aerial vehicles and drones (Intaratep et al. 2016). Although considerable progress has been made in recent decades toward understanding the acoustic sources and noise-production mechanisms specific to a wide range of industrial and engineering flows (Crighton 1975, Ffowcs Williams 1977, Howe 1978, Wang et al. 2006), interest continues to grow in developing novel means to mitigate aerodynamic noise generation that can be translated across many industrial sectors where there may also be a trade-off between stealth and performance.

For over 80 years, researchers have drawn inspiration from nature's silent flier, the owl. The phenomenon of silent owl flight is well acknowledged anecdotally and has been scientifically confirmed by noise measurements of owls in isolation (Kroeger et al. 1972) and in comparison with other birds (Neuhaus et al. 1973, Sarradj et al. 2011). In the context of the owl, the notion of silence implies that prey cannot sense their predator until it is too late to react. Furthermore, many larger owl species such as the barn owl can identify and continuously track their prey in flight by hearing alone (Payne 1971). Therefore, silent owl flight also requires that any aerodynamic noise produced by the owl must not interfere with their acoustical tracking ability. The technological implication is that if the physical mechanisms enabling owls to suppress broadband flow-generated noise can be properly understood at the bird scale, then this understanding could be translated and integrated into new designs for low-speed noise mitigation and control at various speeds and scales. To date, and to the authors' knowledge, no one has engineered an owl-like device that replicates the noise reduction capacity of the owl, and this challenge remains a point of attack for aeroacousticians, fluid dynamicists, and roboticists seeking to recreate owls' silent feat.

This review summarizes research to date into how owls achieve silent flight and how they have inspired nascent noise-reduction technologies in engineering design. Our overview begins with an assessment of owls themselves, including their unique physical attributes and foraging behavior. It is important to note the broad diversity in the size, prey, and specialized adaptations of owl species, and a special effort is made to highlight how some owls may possess but not use (or be able to exploit) the supposed silent aspects used by other owl species. Next, existing noise measurements of owls are reviewed together with a survey of the geometrical details of the predominant wing features thought to produce silent flight. An overview of the standard routes of aerodynamic noise generation in low-speed flows is provided to frame an examination of owl noise suppression in terms of physical mechanisms. Efforts to model the features of owl wings thought

to make them silent are then reviewed and summarized, followed by the noise-reduction technologies these models and owl-related studies have inspired. The review concludes by identifying missing features in the literature that, in the authors' view, are still required to isolate and prove the central noise mechanism(s) that enable broadband aerodynamic noise suppression of the owl, as well as the technological barriers to translating knowledge of owl aeroacoustics into owl-inspired technological innovations.

2. OBSERVATIONS OF THE OWL

We now consider the flight of the owl in the context of using acoustic stealth to silently track and capture prey. First, the diversity of owl species is highlighted with respect to foraging behavior and its connection to bird size, which informs research questions related to the relevance of silent flight mechanisms across the full range of owl species. Second, information from the research literature on the hearing sensitivity of the owl and of the mammalian prey common to larger owl species is presented and compared to the aerodynamic noise measured from live owls and other birds. These measurements demonstrate that owls can suppress self-noise in their most sensitive hearing range while tracking prey acoustically and evading acoustic detection to within a certain closing distance. Lastly, we introduce and discuss the wing attributes historically attributed to owl aerodynamic noise suppression.

2.1. Foraging Behavior

Each owl species has a specific combination of hunting objectives and means of capture, which are not uniform across all owl species. Owls range widely in size, weight, and habitat, features that are coupled to the size and type of their preferred prey. This observation calls into question whether all owl species are indeed silent to their prey or need to be silent.

Larger owl species hunt primarily in a gliding mode on approach, which ends in a thrust toward the prey at the final instant (see **Figure 1**). This behavior is consistent in both lighted (Norberg 1970) and darkened (Payne 1962) conditions, where in the latter case, the owl must make continuous flight path adjustments en route to its prey using acoustical cues. These larger owl species favor mammalian prey indigenous to their habitat, which typically include rodents such as voles and mice. The size of the prey decreases with the size of the owl species, and the foraging behavior also changes for smaller owl species. At body sizes near the boreal (Tengmalm's) owl (*Aegolius funereus*), many owl species begin to pounce on mammalian prey from above without the gliding phase, but acoustical tracking is maintained for these species. For the smallest owl species such as the elf owl (*Micrathene whitneyi*) and pygmy owl (*Glaucidium passerinum*), the prey type shifts from mammals to insects, which are acquired by hawking or pouncing (Johnsgard 2002).

This shift in foraging behavior provokes several critical questions regarding the role of aeroacoustics for owls. For example, are all owl species silent to their prey? If not, do owls need to be effectively silent? Are there similar or different features on large and small owls that might suppress aerodynamic noise? Are these features vestigial for small owls (i.e., does the relevant noise suppression not cut on to be useful at their scale)? Some of these questions are touched upon in this review in the following sections, but these issues remain largely unresolved from a scientific point of view, as the published research literature has principally focused on the noise emitted from larger owl species. The need to compare foraging behavior and noise generation across the size range of owl species presents a ripe opportunity for future cross-disciplinary investigations.

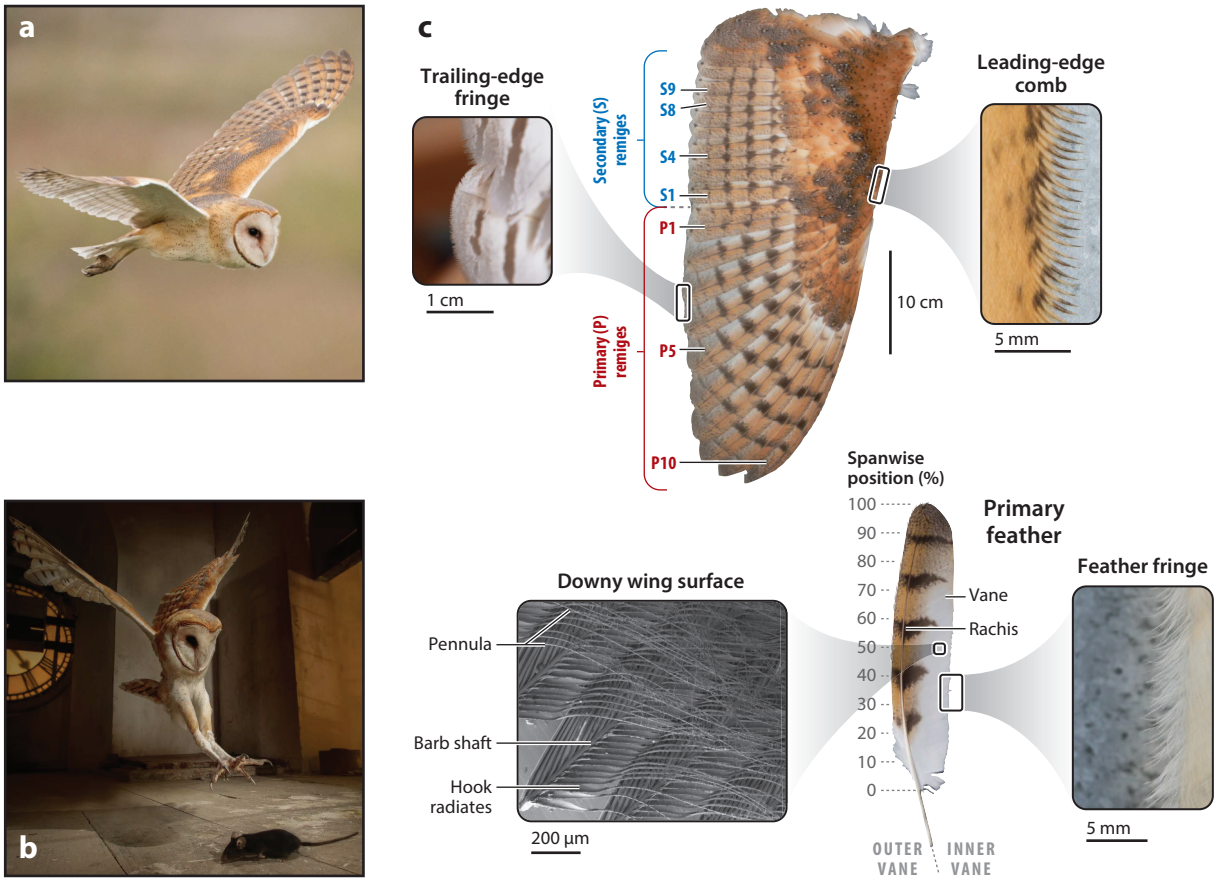

Figure 1

The flight and wing specializations of owls. (*a*) The gliding phase of the barn owl (*Tyto alba*) culminates in (*b*) a wing flare and lunging motion with its talons. (*c*) Physical features at the wing edges and the owl upper-wing surface have been the focus of research efforts to understand their silent flight. Images are adapted with permission from the Slater Museum of Natural History (wing), Ian Davies (gliding owl), Chris Jimenez (owl with prey), Riley Saeger (downy surface), and Christa Neu (feather, leading-edge comb, and fringe).

2.2. Owl Noise Measurements and the Threshold of Hearing

Thorpe & Griffin (1962b) conducted the first acoustic measurements of owls in free flight, whose aerodynamic noise in the ultrasonic frequency range (above 15 kHz) could not be detected by their experimental apparatus. The multiple owl species examined included the scops owl (*Otus scops*), little owl (*Athene noctua*), tawny owl (*Strix aluco*), barn owl (*Tyto alba*), long-eared owl (*Asio otus*), and cayenne owl (*Rhinoptynx clamator*). Ultrasound could not be detected from any of these owl species during gliding flight, in contrast to a broad range of non-owl species of comparable size for which this ultrasonic noise component could be reliably measured. Later comparative measurements by Neuhaus et al. (1973) found that the peak noise from a mallard duck (*Anas platyrhynchos*) occurred near 4 kHz, which lies within the frequency range of maximum sensitivity for humans and owls alike (Konishi 1973). However, the peak noise for the tawny owl (*S. aluco*) occurred within a lower frequency range of 200 to 700 Hz, and its maximum sound pressure was reported to be smaller by a factor of 30 (approximately 30 dB quieter) than the mallard. Additionally, Neuhaus et al. (1973)

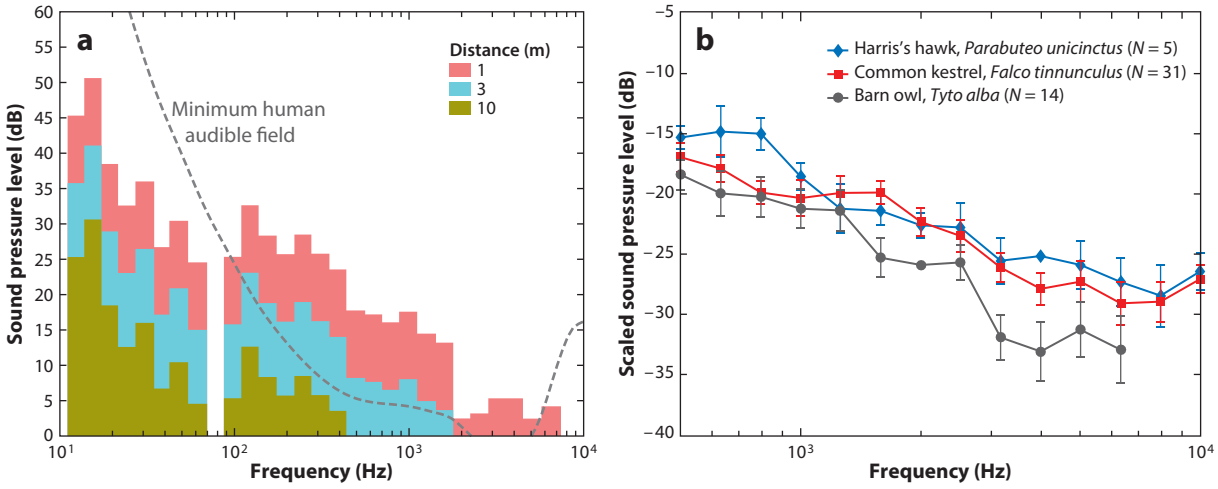

Figure 2

Flyover noise measurements of live owls. (*a*) Sound pressure level measurements by Gruschka et al. (1971) from a single microphone at various distances from the bird, compared against the human threshold of hearing. (*b*) Sound pressure level one meter away for three bird species measured by Sarradj et al. (2011), scaled by the fifth power of the flight speed. The barn owl is notably quieter beyond 1.6 kHz, and the acoustic array could not resolve its signal beyond 6.3 kHz.

reported similar noise levels for both birds in the takeoff phase when the wings are flapped, corroborating Thorpe & Griffin's (1962a,b) observation of a noisier start-up phase.

Gruschka et al. (1971) and Kroeger et al. (1972) carried out flyover noise measurements of a single owl species, the Florida barred owl (*Strix varia alleni*), which was trained to glide through a reverberation room over a single microphone. Their comparison of the owl sound pressure spectrum against the threshold of human hearing indicated that a gliding owl would be effectively silent to a human observer beyond a distance of three meters (see **Figure 2*a***). These measurements are consistent with those of Neuhaus et al. (1973) for the tawny owl, where high-frequency sound is suppressed and the majority of the acoustic energy is contained in frequencies below 1 kHz. However, Konishi (1973) notes that barn owls, for example, are more sensitive to sounds in the 500 Hz to 10 kHz range than humans; for more details on the hearing sensitivity of different owl species, readers are referred to Dyson et al. (1998, table 2). This sensitive frequency range of the owl overlaps with the broadband rustling noises made by prey such as voles, where most of the acoustic energy is in the 1–3 kHz range, but it should be noted that these noises also contain significant frequency content up to 14 kHz (Konishi 1973, figure 3).

Sarradj et al. (2011) conducted a critical assessment of these and other earlier acoustic measurements of live owls against the noise signatures of other birds, citing challenges in attaining consistent and demonstrative results due to lack of flow speed corrections, limitations of the acoustic recording apparatus (single microphone) and of early measurement techniques, and difficulties in promoting natural bird flight to get representative acoustic measurements. Sarradj et al. (2011) compared flyover noise measurements of the barn owl (*T. alba*) against the Harris's hawk (*Parabuteo unicinctus*) and common kestrel (*Falco tinnunculus*) using an acoustic array to produce maps of the acoustic source regions on the birds. The flight speeds of all birds were consistent and were approximately 5 m/s. No significant difference in noise level was observed below 1.6 kHz among all species considered. However, above 1.6 kHz, the owl was substantially quieter than the other birds by 3–8 dB when compared in third-octave bands. **Figure 2*b*** presents these relative acoustic

Strigiformes: the taxonomic order containing all owl species

measurements scaled by the fifth power of the flight speed; the basis for this velocity scaling is detailed in Section 4.1. Above 1.6 kHz, the sound pressure spectrum of the kestrel and Harris's hawk decreases by 10 dB/decade, whereas barn owls have a greater 15-dB/decade roll-off, consistent with earlier live owl measurements where high-frequency content is noticeably absent. Sarradj et al. (2011) noted that their acoustic array was unable to measure the flyover noise of the barn owl at frequencies beyond 6.3 kHz. Since the flight speeds were approximately equal and were considered in the acoustic analysis, Sarradj et al.'s live bird measurements support the hypothesis derived originally from laboratory experiments of fixed-wing specimens (Geyer et al. 2009, 2013) that silent owl flight is a consequence not only of owls' low flight speed but also of their specialized wing adaptations.

These experimental studies underscore the ability of many average- to large-sized owl species to suppress aerodynamic noise above a critical frequency of approximately 1.6 kHz. This frequency range of enhanced aerodynamic noise suppression extends across the sensitive hearing range of humans and owls, as well as the ultrasonic region where the hearing of mammalian prey is keenly sensitive (e.g., see Heffner & Masterton 1980). Consistent results for broadband aerodynamic noise suppression of owl wings in live measurements and fixed wings in laboratory experiments suggest that a single feature or a combination of features of the wing itself is responsible for this noise reduction.

2.3. Wing Attributes

Graham (1934) first identified and reasoned that three wing specializations whose combined appearance is unique to owls may have a physical basis to affect aerodynamic noise generation: a comb of fibers along the leading edge, a compliant trailing-edge fringe, and a velvety down-like material on the upper surface of the wings. Graham interpreted the absence of these wing specializations on fish owls as evolutionary support that these specializations are responsible for silent flight; however, a more rigorous phylogenetic correlation among owl species and these wing features has yet to be carried out to provide scientific support of this speculation. Indeed, features such as the downy upper-wing surface have been observed on other night birds such as frogmouths (Podargidae) and nighthawks (Caprimulgiformes) (Sick 1937, Wagner et al. 2017) but are absent on some owl species (Strigiformes). Nevertheless, Graham (1934) became a focal point for aeroacousticians (cf. Lilley 1998) and biologists seeking to better understand the morphology of these wing attributes and their potential to bring about new mechanisms for aerodynamic noise reduction. Physical measurements of these features and their variations across the wing and across owl species are now surveyed to frame the parameter space occupied by these quiet fliers.

3. PHYSICAL OWL MEASUREMENTS

The observation that owl wing features are not uniform across all species calls into question their roles in aerodynamic noise suppression. For example, **Table 1** indicates a wide variation in wing aerodynamic chord (measured from leading edge to trailing edge) across a representative selection of owl species. The barn owl is the most studied owl species in the academic literature, and their general data for all three wing specializations are presented by Bachmann et al. (2007, 2011, 2012a) and Bachmann (2010). The relationships between these baseline data for barn owls against other owl species are identified in the following sections.

3.1. Leading-Edge Comb

Seminal morphological measurements by Bachmann et al. (2007) using five wings from three different barn owls (*T. alba pratincola*) identified for the leading-edge comb a mean serration length

Table 1 Maximum wing chord lengths of various owl species and their magnitudes relative to an acoustic wavelength at frequency 1.6 kHz in air

Owl species	N^a	Chord (cm)	Wavelengths per chord
Snowy, *Nyctea scandiaca*	4 (2,2)	29.8 ± 2.4[b]	1.39
Great grey, *Strix nebulosa*	4 (2,2)	27.7 ± 7.7	1.29
Great horned, *Bubo virginianus*	7 (3,4)	24.6 ± 2.0	1.15
Barred, *Strix varia*	6 (2,4)	24.4 ± 0.4	1.14
Barn, *Tyto alba*	4 (2,2)	19.0 ± 0.6	0.89
	4	17.1 ± 3.0[c]	0.80
Long-eared, *Asio otus*	4 (0,4)	17.3 ± 0.8	0.81
Burrowing, *Speotyto cunicularia*	6 (4,2)	12.3 ± 0.9	0.57
Boreal (Tengmalm's), *Aegolius funereus*	4 (2)[d]	11.3 ± 0.7	0.52
Northern saw-whet, *Aegolius acadicus*	4 (2,2)	9.84 ± 0.24	0.46
Flammulated, *Otus flammeolus*	2 (2,0)	9.16 ± 0.11	0.43
Elf, *Micrathene whitneyi*	2 (0,2)	8.48 ± 0.19	0.40
Northern pygmy, *Glaucidium gnoma*	8 (6,2)	7.13 ± 0.39	0.33

[a]Number of wing specimens: total (male, female).
[b]Measurements are of spread-wing images from the Slater Museum of Natural History unless otherwise noted. Data are included in **Supplementary Materials**.
[c]Data for mean wing chord reported by Bachmann (2010).
[d]Two wings from a single male specimen and two wings from a specimen of unidentified sex.

Supplemental Material >

of 1.8 mm, a linear density of 18 serrations/cm, and a serration base width of 555 μm with an almost linear taper to the serration tip. Bachmann & Wagner (2011) later carried out the most complete investigation to date on the geometrical details of the leading-edge comb. In their study, six tenth-primary (P10, see **Figure 1**) remiges from five barn owls were measured in static conditions in stationary air. The average overall serration length was 2,670 μm, the separation distance between individual serrations was 575 μm, and the mean upward inclination of the serration at the leading edge was 29°. Consideration of this serration angle and its placement on a gliding barn owl wing indicated that the serrations in flight were inclined almost perpendicularly to the incoming flow. Curvature and thickness distributions of the serrations at various positions on the feathers were also recorded. Detailed measurements across the feathers over 1-cm regions located at the 20%, 40%, 60%, and 80% spanwise positions along the vane (cf. **Figure 1**) revealed that leading-edge serrations at the distal (outboard) part (80% span) of the feather have rounded tips and are the shortest (1,823 ± 239 μm). The central and basal (inboard) serrations have acute tips, are statistically longer, and are longest at the central region (60% span; 2,716 ± 328 μm); this distinction between sharp basal serrations and rounded distal serrations was noted by Sick (1937). The linear spacing between serrations increases with the outward position, where its value when moving from 20% to 80% span varies from 490 to 670 μm, respectively. Spanwise feather positions with a narrower spacing distance had narrower serration base thicknesses and vice versa, i.e., 500 μm at 20% and 650 μm at 80% spanwise locations. A separate study on barn owls by Bachmann et al. (2011) arrived at comparable geometric values and trends in morphological variation across the feather. Furthermore, Roulin et al. (2013) developed a preliminary statistical model of the barn owl using data from 43 male and 50 female specimens that indicated the independence of serration length with sex, age, barb length, vane length, and vane area.

The wealth of available data for the barn owl begs the question of whether or not their serration morphology is representative of all owl species. To address this question, Weger & Wagner (2016) conducted physical measurements of the leading-edge combs of seven different owl species that

covered a range of body sizes and active times of day. The average serration lengths across the species studied ranged from 1 to 3.5 mm, where the serration length generally increased with the size of the owl species. The serrations of the Eurasian eagle-owl (*Bubo bubo*) were significantly longer than the other six species, with serration lengths between 5 and 7 mm. However, they concluded that the serration length is not clearly determined by either the size or activity (i.e., diurnal versus nocturnal) of the owl species and is likely influenced by both factors. Notably, they did not arrive at a definitive result, for example, that nocturnal owls have long serrations and diurnal owls have short serrations. The out-of-plane bending displacement angle of the vane was found to be the best defining characteristic of the serration, where a larger bending angle was prominent for nocturnal rather than for diurnal species. Surprisingly, the correlation between owls' diurnal or nocturnal activity and their serration length was found to be highly variable.

In their discussion, Weger & Wagner (2016) raised the question of why diurnal owls would have serrations at all, under the supposition that serrations are detrimental to aerodynamic performance. With reference to a phylogenetic tree (Wink et al. 2009), they posited that serrations may be a plesiomorphic (shared) characteristic of Strigiformes, but more morphological measurements of other owl species are necessary to support any firm claims about the biological basis for the development and function of serrations comprising the leading-edge combs.

3.2. Trailing-Edge Fringe

Fringe describes the separated barb tips of the inner vane where the hooklets holding the vane together are absent. The fringes on individual feathers together form the frayed trailing edge of the composite wing. Bachmann et al. (2012b) carried out physical measurements of fringes on barn owls (*T. alba pratincola*) using five individual feathers at the inner vane location. This study analyzed five individual feathers from five different wing positions (P10, P5, P1, S4, S9; cf. **Figure 1**) for 25 feathers total. The average length of the fringes ranged narrowly from 2.0 to 2.4 mm in the central feather regions. There was no significant statistical variation across feather types, with the exception of the P10 feather whose mean fringe length was 3.49 ± 0.53 mm. The longest fringes were observed at the central and distal regions of the feather, and the shortest fringes were near the feather base. The mean linear density of fringes ranged from 3.02 to 3.35 per mm, and the variation in linear density across different feather types was found to be statistically insignificant.

With regard to other owl species, Sick (1937) noted that fringes are found on the flight feathers of almost all owls, but the lengths of the fringes vary from species to species. Graham (1934) observed that the fish owl species *Bubo peli* and *Bubo flavipes* have neither fringes nor serrations.

3.3. Downy Wing Surface

The elongated pennula on the upper surface of many owl feathers gives the wing its velvety texture. Klän et al. (2012) likened owl pennula to a surface roughness composed of flexible elements and reported average physical measurements of approximately 200 pennula/mm^2, each with a diameter of approximately 6 μm. For barn owls, Bachmann et al. (2007) determined that the pennula on the inner vane are longer than on the outer vane. The average pennulum lengths on the inner (outer) vanes were $1{,}271 \pm 87.1$ (601 ± 57.5) μm, which are significantly longer than those of a pigeon (*Columba livia domestica*), 136 ± 15.0 (79 ± 6.6) μm. The authors noted that the barn owl pennula are long enough to extend across up to four neighboring barb shafts on the feather vane. Although the pennula are longer for the barn owl than for the pigeon, the density of pennula per unit area is greater for pigeons than for owls, e.g., 152.5/mm^2 versus 99.9/mm^2 on the inner vane of P10, respectively.

Bachmann et al. (2011) analyzed six individual feathers at five feather positions (P10, P5, P1, S4, and S8) at three spanwise locations (25%, 50%, and 75%) along the feather vane. This work furnished quantitative data to corroborate the result that uncovered areas of the vane (i.e., part or all of the outer vane) have a lower pennula density. Also, these uncovered regions of the feather have a lower volumetric porosity and larger angle with respect to the vane surface, which results in a thinner velvet layer. In the uncovered (covered) areas, the pennula densities were 79.4 (84.9) mm^{-2}, the porosity ranged from 0.714 to 0.890 (0.929 to 0.950), and the thickness of the downy layer ranged from 122.3 to 229.7 (310.0 to 497.3) μm. In covered areas, the pennula density is lower, but the structure is thicker and more porous due to the more-upright and longer pennula (Bachmann 2010).

Weger & Wagner (2017) analyzed the pennula on eight wings of the American barn owl (*Tyto furcata praticola*) in gliding position to facilitate a comparison with Bachmann et al. (2007, 2011). In contrast to other studies involving individual feathers, these authors studied the pennulum variation in the total wing surface at four spanwise locations (20%, 40%, 60%, and 80%), with 12 chordwise measurements at each spanwise location. The majority of positions measured had a highly uniform length, with an average value of 793 ± 166 μm. However, the pennula were longer at measurement points closest to the leading edge (chordwise positions of 15% to 20%), with a maximum of 1,053 ± 205 μm at 20% span and 20% chord. These authors speculated that the uniform pennulum length across the wing, with a position-dependent change at the leading edge, is connected to boundary layer control to avoid flow separation. Indeed, the chordwise position of maximum pennulum length is consistent with the location of boundary layer separation on owl-based wing models tested by Klän et al. (2009, 2012) and Winzen et al. (2013).

The consideration of owl pennula morphometric data with fluid mechanics and bird phylogeny raises important questions that will likely require cross-disciplinary research to address. For example, Weger & Wagner (2017) asked that if the purpose of the velvet surface is to mitigate flow separation, why did it not evolve on other bird species? Also, why is the velvet-like surface present on other birds that hunt at night [e.g., nightjars (Sick 1937)], where the prey (insects) are not expected to perceive flight noise? On this point, the question of whether insects react to aerodynamic noise has begun to receive attention (Fournier et al. 2013). Among owl species, Weger & Wagner (2017) reported that the diurnal pygmy owl (*G. passerinum*) does not have elongated pennula to produce a velvety wing surface. They also noted that measurements have been taken on other owl species, where preliminary unpublished data have identified that the pennula of the diurnal little owl (*A. noctua*) and the Eurasian eagle-owl (*B. bubo*) are also longer than the pigeon (*C. livia domestica*), but pennula in the diurnal little owl are shorter than that of two noctural owl species, the barn owl and the Eurasian eagle-owl. These preliminary works underscore the need to collect more data across owl species to better understand the evolution of this wing feature, as well as its potential influence on aerodynamic noise mitigation.

3.4. Owl Flight Parameter Space

A nominal parameter space can now be framed to view silent owl flight from a fluid dynamics perspective. Average flight speeds are on the order of 5 to 7 m/s (Kroeger et al. 1972, Sarradj et al. 2011, Wolf & Konrath 2015), which with reference to **Table 1** leads to a chord-based Reynolds number range of 2.2×10^4 to 1.3×10^5. A representative value for the barn owl is 7×10^4. A flight speed of 5 m/s leads to the small flight Mach number of 0.015. Owl wing features introduce additional length scales: The downy layer is approximately 1 mm thick, and a representative length of both the fringe and leading-edge comb is 2 mm. These features are much smaller than the acoustic wavelength of 1.6 kHz in air, 21 cm; however, this acoustic wavelength can be either larger

or smaller than the wing chord over the range of owl species (cf. **Table 1**), which has implications for acoustical modeling efforts and physical interpretation. Of course, other dimensionless groups may be constructed from the physical measurements surveyed here, as well as from additional fluid dynamics data particular to a given flight scenario, such as the boundary layer thickness. Owls fly with modest angles of attack in level gliding flight, and many of the principal mechanisms for aerodynamic noise generation can be analyzed for wings at zero angle of attack. These physical mechanisms and their fluid dynamical basis are reviewed in the following section.

Acoustical compactness: the spatial extent of a sound source on the scale of the acoustic wavelength; acoustically compact sources are sufficiently small that retarded-time variations across the source, for a given observer, can be neglected

4. MECHANISMS OF NOISE GENERATION

4.1. Origins of Turbulence Noise

Aerodynamic noise generation in low–Mach number flow results from the conversion of rotational hydrodynamic kinetic energy, often in spatially localized regions of turbulence, into longitudinal sound waves of wavelengths considerably longer than the length scale of the local turbulent flow itself, which are then heard by an observer in the far field (Howe 2003). Lighthill (1952) pioneered the prediction of aerodynamic noise by rearranging the (Navier–Stokes) equations of fluid mass and momentum into the form of a single wave equation for the density $\rho(\mathbf{x}, t)$, which is forced by the fluid stress within the turbulent source region. Specifically, Lighthill showed

$$\frac{\partial^2 \rho}{\partial t^2} - c_0^2 \nabla^2 \rho = \frac{\partial^2 T_{ij}}{\partial x_i \partial x_j}, \qquad 1.$$

where T_{ij} is the famous Lighthill stress tensor that in low–Mach number flow is approximated by the Reynolds stress $\rho u_i u_j$, $\mathbf{u}$ is the fluid velocity, and c_0 is the speed of sound in an otherwise quiescent medium. For low-speed flows, a turbulent eddy may often be modeled compactly as a point quadrupole source, so that the far-field density fluctuation ρ', i.e., the noise, is given by

$$\rho'(\mathbf{x}, t) = \frac{1}{4\pi c_0^2 |\mathbf{x}|} \frac{\partial^2}{\partial x_i \partial x_j} \int T_{ij}(\mathbf{y}, t - |\mathbf{x}|/c_0)\, \mathrm{d}^3\mathbf{y}. \qquad 2.$$

Note the single retarded time $t - |\mathbf{x}|/c_0$ appearing in the source distribution, indicating the assumed acoustical compactness of the source on the scale of the typical acoustic wavelengths involved.

In low-speed flow (but definitely not in high-speed flow) quadrupoles are extremely inefficient acoustic radiators compared to progressively stronger dipole sources (resulting from unsteady forces, e.g., the unsteady lift on a fluttering airfoil) and monopole sources (resulting from volumetric changes, e.g., a bursting bubble) typical in acoustics problems. To see this specifically, we denote a typical turbulent length scale and timescale by l and ω^{-1}, respectively, implying an acoustic wavelength λ scaling as l/m, where we can identify $m = l\omega/c_0$ as the Mach number of the turbulent flow. Taking the limit $m \ll 1$, we see $\lambda \gg l$ straight away, confirming the compactness of the source region on the scale of the acoustic wavelength. Lighthill (1952, 1954) showed directly from Equation 2 that the density fluctuation scales with the fourth power of the Mach number. This scaling is made up of two factors of m from the quadrupole term, and another factor of m from each of the two spatial derivatives, given that the observation position appears in the time argument of the quadrupole thanks to the assumption of perfect source compactness. Therefore the acoustic power emitted from free-field turbulence in low-speed flows scales as m^8. In comparison, the acoustic power from dipoles and monopoles scales as m^6 and m^4, respectively. For small m we might expect that the free-field turbulence noise is most likely dominated by other, more efficient, noise sources.

The weak acoustic emission of free-field turbulence at low speeds is significantly strengthened by its interactions with solid bodies. Curle (1955) demonstrated that a turbulent quadrupole close to a solid body produces a far-field acoustic power scaling as m^6, perhaps not surprisingly since the presence of the turbulence will induce an unsteady force on the body corresponding to a distribution of surface dipoles. However, more surprisingly, Ffowcs Williams & Hall (1970) demonstrated that even more efficient noise generation occurs when the turbulence is close on the wavelength scale to a sharp edge, as it would be when a turbulent boundary layer passes over the wing trailing edge. The conversion of the local hydrodynamic motion into sound is enhanced by the geometric singularity at the edge, leading to the acoustic power scaling as m^5, which is m^{-3} louder in a scaling sense than a free-space turbulent eddy. More precisely, this scaling arises from the effect of the presence of the trailing edge, for which the equivalent version of Equation 2 contains an additional factor $(\omega r_0)^{-1/2}$, where r_0 is the distance of the turbulent source from the trailing edge. Once the two spatial derivatives have been completed, this leads to a dominant term containing an extra factor $(\omega r_0)^{-3/2}$, and hence an additional factor $m^{-3/2}$ compared to the Lighthill free-field result.

4.2. Biological Noises

The complex construction of bird wings can introduce additional noise sources other than classical trailing-edge noise. Air passing through compliant feathers can lead to aeroelastic flutter, which generates a buzzing or chirping noise observed for other birds (Clark & Prum 2015) and has been postulated as a part of the courtship ritual for small-eared owls (Dubois 1924). Many bird species produce a variety of nonvocal (mechanical) sounds due to feathers clapping either together or against the body, as well as from feather-to-feather rubbing (Bostwick & Prum 2003, Clark 2016). The elongated pennula on the upper surface of owl feathers likely reduce the noisy frictional contact between feathers and suppress this potential biological noise mechanism (Sick 1937, Hertel 1963). Bachmann et al. (2012b) demonstrated that the fringe at the trailing edge of each owl feather fits into the grooves of the neighboring feather to promote a stable wing shape that is further resilient to flow-induced feather-rubbing noise. However, the details of this friction noise for owls remain qualitative, such as the casual demonstration done with feathers in hand by Graham (1934).

5. MODELING OF WING FEATURES

5.1. Trailing-Edge Noise

We have already noted the famous Ffowcs Williams & Hall (1970) result that noise resulting from the scattering of a turbulent boundary layer passing over a sharp rigid edge potentially dominates other noise sources in terms of Mach number scaling. The obvious question of how this effect might be reduced by suitable emendation of the geometrical or material properties of the trailing edge has received a great deal of attention. One of the first such investigations was made by Crighton & Leppington (1970), who considered the simplified case of a semi-infinite compliant surface (precisely, one in which elastic effects are weak, so that the surface normal velocity is related to the local pressure by an impedance condition). The magnitude of the scattering, it turns out, is then determined by the level of fluid loading (specifically, the ratio of fluid mass within one acoustic wavelength of the plate to the mass per unit length of the plate); in cases of low fluid loading (as would often be the case for a heavy structure in air), the rigid-plate m^5 result is regained, but for heavy fluid loading (as would often be the case in water or for a light structure and low-frequency sound in air) the trailing edge is not an effective scatterer and the ordinary m^6

scaling for a surface without an edge is regained. This result reveals the possibility of reducing the efficiency of trailing-edge scattering by essentially making the jump in boundary conditions experienced by turbulent eddies passing over the trailing edge less severe. More sophisticated models of plate compliance have since been completed, for instance using thin-plate theory to include elasticity (e.g., Cannell 1975, 1976; Howe 1992, 1993).

Plate porosity has also been studied as a method for reducing trailing-edge noise. For instance, Howe (1979) considered the sound produced by a point vortex convecting over a trailing edge with and without perforations and showed that the presence of holes significantly reduces, on a decibel scale, the amplitude of the impulsive far-field pressure peak associated with the abrupt change in boundary conditions. In a different direction, the use of small sections of porous material has been shown to reduce trailing-edge noise from multielement high-lift airfoils, including early experiments (Fink & Bailey 1980) and computations (Khorrami & Choudhari 2003). The latter revealed that the porous material may well act in several ways, not only in reducing the strength of edge scattering but also in modifying the hydrodynamic noise source itself (e.g., by reducing the strength of coherent vortex shedding from the finite-thickness trailing edge).

Combining both elasticity and porosity (i.e., a poroelastic trailing edge) seems especially relevant as a simplified representation of the owl trailing-edge fringe, and a detailed study was completed by Jaworski & Peake (2013). One key question to ask is, How is the Mach number scaling affected by poroelasticity? In other words, can we modify the trailing edge in such a way as to eliminate the potentially troublesome m^5 scaling? The effect of porosity is governed by a dimensionless parameter δ, which is proportional to $\alpha_H c_0/(\omega R)$, where α_H is the open-area ratio, ω is the frequency, and R is the linear dimension of the pores: For $\delta \gg 1$, (i.e., high porosity) the scaling is m^6, whereby the trailing-edge effect is eliminated and the Ffowcs Williams (1972) scaling for an infinite perforated sheet is recovered, while for $\delta \ll 1$ (i.e., low porosity), the m^5 rigid edge scaling is found. Full results are presented in **Figure 3*a***, in which we plot the Mach number index (i.e., n, where acoustic power scales as m^n) against a nondimensional frequency Ω, using parameters that mimic the polypropylene brush experiment of Herr (2007). We see a predicted velocity scaling m^n in the range $4.5 < n < 5$ in the frequency range of interest for the owl (1.6–10 kHz, or $0.1242 < \Omega < 0.3104$ in nondimensional terms), which agrees with Herr's measurements. Of course, this has not had the effect of eliminating the trailing-edge m^5 scaling for the owl, but there is the suggestion that scalings of m^6 or even m^7 are achievable at the lower end of human hearing, especially when elasticity is included. Noise measurements by Geyer et al. (2010) on airfoils made of only porous materials indicated that velocity exponents greater than 5 can be realized, in agreement with the porous-only curve in **Figure 3*a***, for which we have $5 < n < 6$. However, the value of n is of course not the only factor that determines the sound level—there must be a (material-dependent) constant of proportionality as well. When we look at the variation of the actual sound pressure level against dimensional frequency (**Figure 3*b***), we see that significant overall reductions are indeed achieved compared to the rigid edge, even in the frequency range of most interest for the owl. It is especially noteworthy in **Figure 3*b*** that the poroelastic plate outperforms pure elastic and porous cases across the whole frequency range.

Of course, the model of Jaworski & Peake (2013) contains several simplifications, not least of which is the semi-infinite plate geometry. With this in mind, Cavalieri et al. (2016) completed numerical computations using the boundary integral technique for a finite-chord poroelastic airfoil, and again they found substantial improvements compared to the rigid case. (One insight not available from the semi-infinite chord case was that porosity appears most effective at reducing sound at scales comparable to the airfoil chord, while elasticity is more effective at shorter wavelengths—the two therefore combining to yield reductions over a broad spectrum.) Further numerical work by Pimenta et al. (2018) showed that including additional spanwise features, such

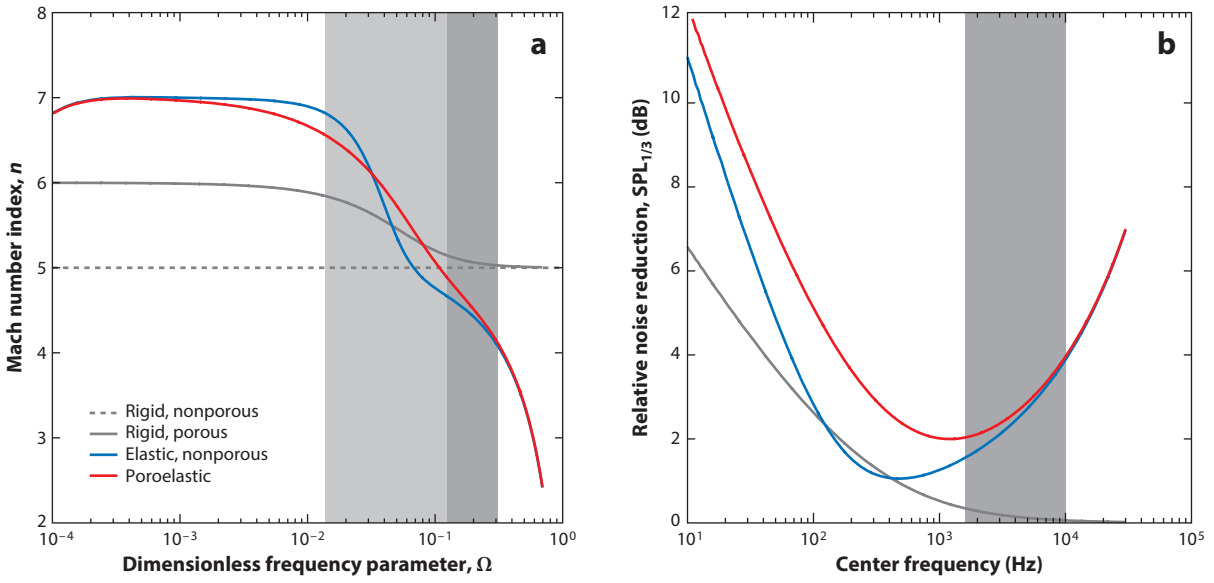

Figure 3

Dependence of quadrupole edge noise scaling and reduction on frequency. (*a*) The exponent n of the Mach number plotted against the frequency parameter $\Omega = (\omega/\omega_c)^{1/2}$, where ω_c is the coincidence frequency $(m_p c_0^4/B)^{1/2}$, m_p is the plate mass per unit area, B is the plate bending stiffness, and c_0 is the speed of sound of the surrounding fluid. (*b*) Sound pressure level (SPL) reduction for various edge conditions relative to rigid nonporous trailing-edge noise. Results are reported in third-octave averages as a function of the center frequency over the nominal range of human hearing. The shaded region in panel *a* indicates the human range of hearing of humans up to 10 kHz, and the darker regions denote the frequency range of interest to the owl, 1.6–10 kHz. Figure adapted with permission from Jaworski & Peake (2013).

as a swept trailing edge and trailing-edge serrations, can reduce scattering even further, presumably by introducing effects that reduce spanwise coherence and thereby enhance (destructive) interference from sources along the trailing edge. In a different direction, Kisil & Ayton (2018) used an iterative method to solve the matrix Wiener–Hopf problem of scattering by a semi-infinite rigid plate with a finite-length porous appendage. The interesting additional feature here is that the rigid–porous junction acts as a second place where boundary layer turbulence can be scattered. The resulting sound interferes with the trailing-edge sound to produce an overall acoustic field that is louder than that from a porous trailing edge alone and that depends on both the porosity and the frequency. We can therefore conclude that chordwise noncompactness effects are an important feature when trying to predict trailing-edge noise for a realistic configuration.

As a final note in this subsection, much of the work we have described is concerned with ways to reduce the efficiency with which some given turbulent flow is converted into sound by the trailing edge, rather than with how the turbulence itself can be modified for low noise. For a rigid NACA (National Advisory Committee for Aeronautics) 0012 airfoil, Brooks et al. (1989) completed an exceptionally wide range of experiments at varying flow conditions to produce correlations and scaling laws as functions not only of flow Mach number but also of, among other things, Reynolds number and angle of attack. In fact, they identified other mechanisms for generating trailing-edge noise in addition to turbulence passing over a sharp trailing edge, including coherent vortex shedding that is likely to be important at lower Reynolds numbers and higher angles of attack and tip noise. In order to fully understand trailing-edge noise for a poroelastic airfoil, we believe that the sort of experimental campaign completed by Brooks et al. (1989) would be invaluable. Of course, it

Spanwise coherence: the extent to which broadband acoustic sources along the wing span are correlated with each other and therefore add constructively

Wiener–Hopf technique: an advanced mathematical technique for solving multipart boundary value problems

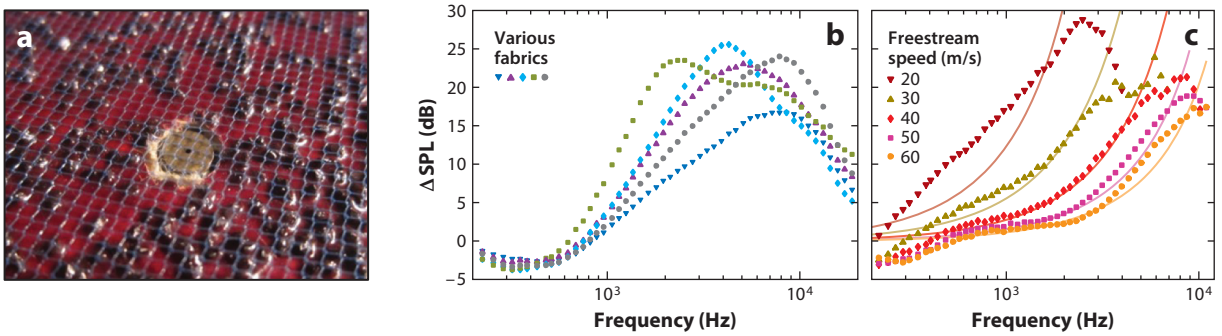

Figure 4

Reduction of surface pressures on a rough surface using suspended canopies of flow-aligned structures. (*a*) A fabric canopy suspended over sandpaper roughness with a surface-mounted microphone. (*b*) Attenuation of surface pressure fluctuations for each canopy over 3-mm roughness at a freestream speed of 60 m/s. (*c*) Comparison of experimentally measured surface pressure attenuation (*symbols*) at several freestream speeds against theoretical shear-sheltering predictions (*solid lines*). Results are presented in terms of sound pressure level (SPL) attenuation in decibels. Panels adapted with permission from (*a*) Clark et al. (2017) and (*b*,*c*) Clark et al. (2016).

might seem that such an investigation would require variation of an unrealistically large number of parameters based on geometry and material properties, but we do believe that the sort of theoretical investigations described here could be used to limit the size of the parameter space required!

5.2. Shear Shielding for Roughness Noise

To elucidate the role of the downy coating on the owl wing, Clark et al. (2016) conducted a series of experiments on the effect on noise and unsteady surface pressure of a fabric canopy suspended above a rough surface in flow. The presence of the canopy on the far-field noise was found to have a marginal effect at best (although, at very high frequencies, fibers aligned transverse to the flow introduced extra vortex-shedding noise). However, the canopy had a dramatic effect on the surface pressure spectrum, attenuating up to 25 dB at peak frequency (see **Figure 4*b***). Of the five fabrics used for the canopy, four had an open-area ratio of around 70%, while one (**Figure 4*b***, square symbols) had a denser weave with approximately 40% open area. One possible explanation for this striking behavior lies in shear sheltering as a mechanism to suppress transverse fluid perturbations: In analogy to common models of forest canopies (see Finnigan 2000), the drag exerted by the canopy might retard the flow to produce an inflectional mixing layer profile that is Kelvin–Helmholtz unstable. The Kelvin–Helmholtz instability leads to exponential growth of velocity perturbations in the flow direction, accompanied by an exponential decay in the transverse direction, i.e., above and into the canopy region, exponentially reducing the pressure footprint on the wall from disturbances propagating above the canopy. Clark et al. (2016) investigated a simple theoretical model of this process, considering waves of fixed frequency propagating in a linear shear profile, and we see in **Figure 4*c*** that good agreement can be found between experimental and theoretical attenuation curves using appropriately chosen values for the shear layer width and strength. More detailed theoretical models of this phenomenon are certainly required.

5.3. Leading-Edge Noise

The arguments that led Ffowcs Williams & Hall (1970) to predict the importance of trailing-edge noise due to the abrupt change in geometry apply equally to the amplification of noise by

turbulence in the presence of an airfoil leading edge. Of course, the difference here is that for the leading-edge interaction the turbulence must originate upstream (perhaps being present as atmospheric disturbances) rather than be created through boundary layer transition en route to the trailing edge. A detailed calculation by Myers & Kerschen (1995) included the effects of airfoil incidence; they considered essentially two-dimensional disturbances, for which the leading-edge noise scales as m^4, which is the same as the analysis of Ffowcs Williams & Hall (1970) in two dimensions.

One feature of leading-edge noise not present at the trailing edge is the fact that, when viewed in the frame of the airfoil, upstream turbulence convecting at the freestream speed must be rapidly decelerated to zero as it approaches the leading-edge stagnation point over a length scale corresponding to the airfoil nose radius. This rapid change in the local mean flow stretches turbulent eddies significantly in the streamwise direction, leading to modification of both the surface pressure and the far-field sound spectra. Results computed by Ayton & Peake (2016) for an elliptic airfoil at zero incidence show good agreement with experiments at long and short length scales. Further analytical and experimental work by Ayton & Chaitanya (2017) extended this to a much larger range of airfoil nose shapes, and they concluded that, for the low speeds and high frequencies of interest for the owl, blunting the leading edge tends to reduce the far-field sound. However, we feel that the precise details of the flow field close to the wing (for instance, accounting for the flow distortion of the leading-edge comb) would need to be included if one were to make realistic predictions of what, if any, noise would be generated by an owl flying into small-scale turbulence (even if one were able to quantify that turbulence in the first place).

Finally, in this subsection we mention the work of Geyer et al. (2017), who conducted wind tunnel aerodynamic and acoustic measurements on specimen owl wings with and without the leading-edge comb. In common with much earlier work by Kroeger et al. (1972), Geyer et al. found that the presence of the comb does not seem to have a clear and consistent effect on flight noise at low angles of attack. However, these researchers found that at high angles of attack, as might occur in the very final stages of the swooping motion as the owl attacks its prey, the noise is noticeably lower (by an order of 3 dB) when the comb is present. Moreover, they showed that the presence of the leading-edge comb appears to prevent the formation of a strong noise source near the wing tip. Whether such an effect is present on a live owl remains an open question. However, from Brooks et al.'s (1989) experiments on the NACA 0012 airfoil, we know that blade tip effects can be at least comparable to the trailing-edge noise from the rest of the blade span in cases where there is a strong tip vortex [see figure 91 of Brooks et al. (1989), where the geometric angle of attack is on the order of 11° and the tip vortex is therefore expected to be strong]. The noise mechanism assumed by Brooks et al. is the same as that suggested by George et al. (1980) in that the tip noise is generated by the turbulence contained within the tip vortex core convecting over the sharp wing tip side and trailing edges. Bringing this all together, it is credible that the leading-edge comb may play a role in reducing spanwise flow variations due to separation at high angles of attack, thereby reducing the strength of the tip vortex and the associated tip noise.

5.4. Coupled Interactions Between Wing Features

Most research carried out to date on owl wing adaptations has considered that wing adaptations act independently. However, the leading-edge comb and velvety down material can in principle change the boundary flow over the wing, most importantly its spectral content. The spectral content of the boundary layer turbulence at the rear of the wing determines the content of the trailing-edge noise; therefore, trailing-edge noise is inherently dependent on upstream conditions.

Any positive or negative effects from upstream flow features on trailing-edge noise must first be able to persist until the trailing edge is reached. The recovery of flow perturbations is generally

longer when transitioning from a flow state with excess shear stress in the boundary layer (such as a rough-to-smooth wall surface transition), rather than the other way around for a boundary layer adjusting from a smooth to a rough wall surface (Antonia & Luxton 1972, Smits & Wood 1985). In contrast, leading-edge features such as combs or vortex generators on wings may introduce coherent structures that evolve and encounter the trailing edge, and experimental measurements are needed to discern these interactions on the noise generation and aerodynamics of wings. Rao et al. (2017) demonstrated that for a flat plate at a 20° angle of attack, the flow from the leading-edge serrations can reduce trailing-edge noise, albeit at a low chord-based Reynolds number (5×10^3). However, recent coordinated analytical and experimental work by Lyu et al. (2019) at higher Reynolds numbers of more practical aerospace interest (6.3×10^5) has shown how the shape of the leading edge can both affect the leading-edge noise due to a turbulent inflow and suppress high-frequency turbulence noise from the leading edge that lies in the self-noise frequency range typically associated with the trailing-edge noise mechanism.

6. BIOLOGICALLY INFORMED TECHNOLOGIES

Wing attributes of the owl have led to an exploration of various wing design strategies to suppress aerodynamic noise. In many engineering applications, especially in aerospace and energy sectors, these innovations must be able to reduce noise while maintaining an aerodynamic performance standard or an acceptable trade-off between a diminished performance metric and noise reduction. At present, many of the wing or blade designs connected to the alleged silent wing features of owls in the previous section continue to be the subject of intense research interest into the basic physical mechanisms responsible for noise suppression and their robustness to variations in operating conditions. In the end, all candidate noise reduction technologies must be able to buy themselves onto the engineering system of interest (such as an airplane or wind turbine) by creating an economic incentive to cover and exceed the cost of design, manufacturing, and maintenance of new technologies.

6.1. Leading-Edge Serrations

Hersh et al. (1974) first explored the use of leading-edge serrations for noise suppression with acknowledgment of the owl wing adaptation. These serrations were extensions placed at different positions near the leading edge of a NACA 0012 airfoil, which were mounted flush or at a fixed angle with the airfoil surface. The flush-mounted serrations (i.e., a leading-edge trip) yielded the greatest noise reductions in their study for both fixed and rotating blades, where their most useful effect was the elimination of tonal noise due to wake vortex shedding. Broadband noise reductions of approximately 3–5 dB were also noted at high angles of attack corresponding to airfoil stall.

Aeroacoustic measurements of leading-edge serrations have been performed on (flat) sawtooth, wavy, slitted, and multiple-wavelength edge designs, as well as three-dimensional and hybrid sawtooth-slitted edge designs. The broad design space and range of Reynolds numbers have generally precluded the identification of best practices for predictive leading-edge noise suppression. However, Lyu et al. (2016) and Lyu & Azarpeyvand (2017) identified destructive acoustic interference between serrations as a key mechanism for serrated-edge noise reduction. Turner & Kim (2017) carried out inviscid computational simulations of a vortex interaction with a flat, wavy edge to discover the importance of the local horseshoe vortex system generated by the serration and its effect on the acoustic source strength at the serration root location. The consistency of wall pressure spectra on the serrated edge but different noise results in the acoustic far field led them to support the hypothesis that the propagation of the scattered acoustic waves

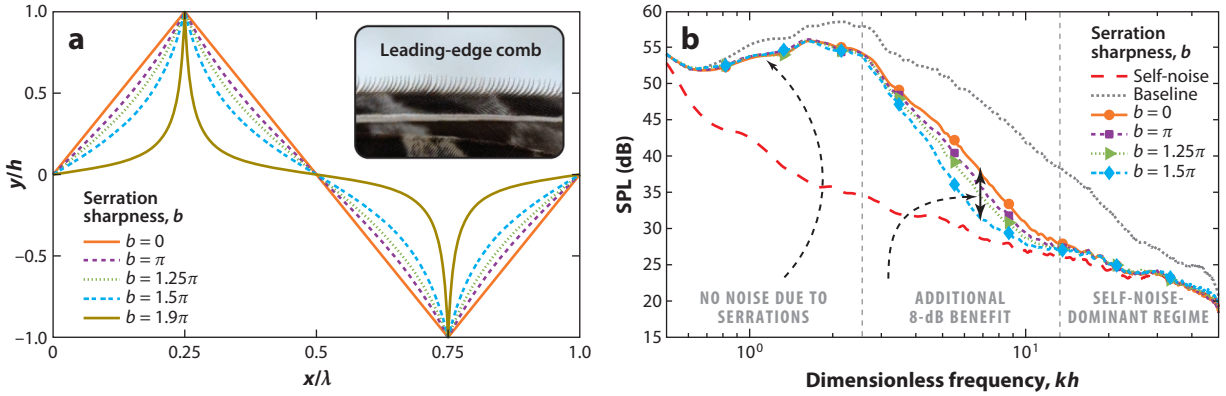

Figure 5

Aerodynamic noise suppression from leading-edge serrations and its dependence on geometry. (*a*) Serration geometries without stationary points are necessary to maximize leading-edge noise reduction. The sharpness of the serration with height h and wavelength λ is parameterized by b. (*Inset*) The pointed leading-edge comb of a long-eared owl. (*b*) Experimental measurements of sound pressure level (SPL) in the acoustic far field for a flat plate at zero angle of attack as a function of nondimensional frequency, with acoustic wave number k and height h. "Self-noise" refers to a serrated case ($b = 1.5\pi$) without upstream grid turbulence, and "baseline" refers to a straight leading edge case ($b = 0$) with grid turbulence. Grid turbulence intensity is 2.5%, with an integral length scale of approximately 6 mm. These serration geometries produce up to 8-dB noise reduction and the removal of leading-edge noise in the self-noise-dominant regime. Figure adapted with permission from Lyu et al. (2019).

is an important mechanism for serrated edges. Chaitanya et al. (2017) determined experimentally that the optimum (sinusoidal) edge wavelength is approximately four times the integral length scale of the incoming turbulence. At this wavelength, the acoustic sources located in the serration trough transition from coherent excitation to just becoming incoherent, which holds for both the flat plate and real airfoil geometries tested. The pursuit of optimal serration designs led Lyu et al. (2019) to determine analytically that thin, pointed serrations yield the greatest noise reduction, which is supported by companion measurements and is shown in **Figure 5*b***. It is tempting to compare these optimized shapes to the leading-edge comb of the owl (see **Figure 5*a***). These recent high-quality research articles integrating mathematical analysis, aeroacoustic measurements, and computational simulations lead one to believe that yet more critical physical insight into serrated edges is still to come from such coordinated efforts.

6.2. Porosity of Aerodynamic Planforms and Edges

Trailing-edge noise represents the minimum noise level possible for airframes and moving blades. Therefore, modifications to the trailing edge have attracted considerable interest as a means to suppress turbulence noise arising from edge scattering. As described previously in Section 4.1, edge noise is caused by the sharp acoustic impedance discontinuity experienced by turbulent eddies as they move from being over the airfoil surface (no penetration) into the wake (pressure release). The effect of this discontinuity may be softened by a porous edge or extension, whereby the transition in the wall boundary condition is gradual. Hayden (1976) identified several additional classes of edge design to achieve effective porosity gradients over a finite region near the trailing edge: a uniformly porous edge with varying thickness, a porous airfoil surface with single or multiple internal cavities, and a solid, slitted (serrated) edge. Experimental application of his variable-impedance edge design to a depressed trailing-edge flap with upper-surface blowing demonstrated a 6-dB reduction at its low-frequency peak and an approximately 3- to

Beamforming: an experimental technique to identify and characterize noise sources

6-dB reduction at higher frequencies relative to the untreated flap. Herr & Reichenberger (2011) found similar levels of broadband noise reduction (3–4 dB) for airfoils with hollow trailing edges covered by a porous mesh or surface, and this acoustic benefit diminished with increasing angle of attack. Furthermore, certain configurations and porous materials were found to generate excess noise at high frequencies. Optimization of the porosity distribution for maximum noise reduction was not carried out in these works, but such optimal distributions have been pursued numerically by Zhou et al. (2018) using discrete adjoint methods and large-eddy fluid dynamics simulations.

More recent experimental acoustic studies examined the effects of partial airfoil porosity at the trailing-edge section only (Geyer & Sarradj 2014) and of airfoils constructed entirely from a uniformly porous textile (Geyer et al. 2010); aerodynamic noise and force measurements were conducted in both studies. These investigations demonstrated that small regions of porosity near the trailing edge are effective at suppressing aerodynamic noise generation in the sensitive range of human audition. This phenomenon can be understood on dimensional grounds: The maximum wavelength of the turbulence noise to be suppressed should be on the order of the porous extension, as anticipated by edge scattering theory (Ffowcs Williams & Hall 1970, Crighton & Leppington 1970).

The observation that the owl wing permits through-flow under certain flight conditions (Kroeger et al. 1972) invites the consideration of porosity for both acoustical and aerodynamic effects, as was noted by Hayden et al. (1972) and Hayden (1976). This acoustic–aerodynamic tradeoff has motivated recent analytical investigations by Iosilevskii (2011, 2013) to predict the fluid forces on airfoils in steady flow that have finite trailing-edge regions of uniform porosity. Hajian & Jaworski (2017) generalized this result and determined in closed form the aerodynamic loads on an airfoil with any Hölder-continuous porosity distribution, which may be further extended for unsteady motions (Hajian & Jaworski 2019). Numerical aeroacoustic solvers, such as those developed by Cavalieri et al. (2016) and Pimenta et al. (2018), now permit the acoustic effects of porous wing planforms and other effects such as wing elasticity. However, a detailed understanding of the acoustic effects of variations in porosity and elasticity along the airfoil chord and particularly near the edges is lacking and requires investigation. Moreover, the addition of finite elastic regions or edge extensions to a wing or airfoil in a flow introduces the possibility of flutter instability (Kornecki et al. 1976, Dowell et al. 2004), which would likely eliminate any potential performance gains and would need to be considered in practice.

6.3. Elastic Trailing-Edge Brushes

To emulate the owl fringe structure, Herr & Dobrzynski (2005) installed elastic brushes to the trailing edge of a flat plate model to weaken the turbulence noise scattering mechanism there. Beamforming acoustic measurements showed that the elastic brushes are most effective at mitigating bluntness noise (caused by vortex shedding at the trailing edge) for chord-based Reynolds numbers of industrial interest (10^6 to 10^7). They made an argument similar to Hayden (1976) for porous edges that the brush extensions affect the local flow field of the turbulent trailing-edge source region. Since beamforming does not allow one to interrogate the turbulent source region, this hypothesis could not be tested.

Herr (2007) later demonstrated that trailing-edge brushes are also effective when applied to realistic airfoil geometries with finite thickness. In her study, the brushes with the smallest spanwise spacing (<0.1 mm) yielded the best noise reduction, further supporting the hypothesis that the brushes are most useful when behaving like an effective porosity with local hydrodynamic energy absorption. The greatest relative sound pressure level reduction occurred at the lowest frequency measured (1.25 kHz), where a stiff brush reduced the noise level by approximately 3 dB

and a flexible brush by an additional 3 dB; these noise-reduction results are consistent with those found by Finez et al. (2010), whose flexible trailing-edge brushes furnished an approximately 3-dB noise reduction below 2 kHz. Noise reduction decreases uniformly with increasing frequency until 16 kHz, at which point the brush trailing edge yields the same noise level as a rigid, impermeable edge. This gradual transition as a function of frequency is consistent with the model predictions by Jaworski & Peake (2013), whereby the noise from a porous edge degenerates to that of an impermeable edge at sufficiently high frequencies, as determined by the details of the edge porosity.

6.4. Surface Design for Turbulence Noise Control

Measurements by Clark et al. (2016) for flow noise past porous veils over rough walls indicated the design strategy of aligning the physical members of the canopy with the flow direction. In this manner, the transverse lift of turbulence would be accomplished while minimizing roughness noise generated by any fibers misaligned with the flow. This strategy led Clark et al. (2015, 2017) to develop streamwise-oriented fin and rail surface structures, termed finlets. In contrast to another device with a similar name, riblets (Walsh 1983, Choi et al. 1993), which act very near the wall to effect drag reduction (typical height and spacing of 10–15 wall units), finlets are comparatively much larger (10–100% of the boundary layer thickness) and therefore manipulate the whole boundary layer. When attached to a stationary DU96-W180 wind turbine airfoil section, the placement of (rigid) finlets directly upstream of the trailing edge modifies and pretreats the boundary layer before it is scattered by the trailing edge (see **Figure 6**). A broadband reduction in aerodynamic noise of up to 10 dB is achieved over a broad range of angles of attack, where the noise reduction is maximum at the zero-lift condition and smoothly diminishes to approach the untreated noise level near aerodynamic stall (see **Figure 6*a***). Parametric studies of the finlet height demonstrated the importance of the cutting of the boundary layer to decorrelate the spanwise turbulence, which is a known driver of trailing-edge noise (Amiet 1976). The decorrelation mechanism hypothesis was also supported by varying the finlet spanwise spacing (pitch), where smaller pitch reduces the maximum correlation length scale that can persist to the trailing edge to be scattered. However, a lower limit on the pitch exists, where the finlets act like a blunt trailing edge and produce low-frequency noise due to vortex shedding. Force measurements on the treated and untreated airfoil show that the lift characteristic is not negatively affected, and the

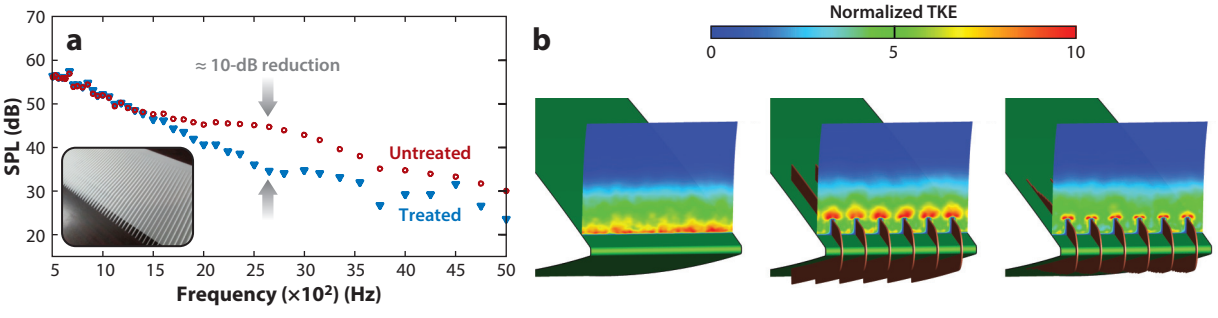

Figure 6

Finlet surface treatments and their effects on the local flow and trailing-edge noise. (*a*) Finlets installed upstream of the trailing edge demonstrate up to 10 dB of broadband noise reduction over an untreated DU96-W180 airfoil section. (*b*) Finlets elevate the maximum turbulent kinetic energy (TKE) in the boundary layer away from the trailing edge. Note that the entry region of the finlets has a persistent effect on the flow near the trailing edge and can become a dominant noise source. Panels adapted with permission from (*a*) Clark et al. (2017) and (*b*) Bodling & Sharma (2019b).

modest increase in drag is commensurate with the amount one would expect from the increase in wetted surface area due to the installation of finlets.

Later work by Clark (2017) and Millican et al. (2017) proposed that, in addition to the boundary layer decorrelation mechanism, the finlets lift up the boundary layer turbulence to diminish the scattering efficiency of high-frequency turbulent eddies at the trailing edge. Bodling & Sharma (2019a) confirmed with high-order computational simulations the importance of this shear sheltering effect, where the regions of high turbulent kinetic energy are localized to the tops of the finlets and away from the airfoil trailing edge. These and complementary simulations by Bodling & Sharma (2019b) shown in **Figure 6*b*** demonstrate the importance of the finlet entry region, which can emerge as its own noise source and effectively nullify any trailing-edge noise reduction benefit.

It should be noted that surface architecture designs to date have been largely exploratory, and no rapid means to optimize their design under desired hydrodynamic (drag) or acoustic performance constraints has yet been applied. Crucially, the surface has a strong effect on the local flow, and such a scheme must be able to connect details of the turbulent flow to the structure of the surface. Recent developments in low-order modeling such as the resolvent analysis (Sharma & McKeon 2013, Chavarin & Luhar 2019) may prove useful in the search for optimal surface designs for a particular scenario, provided that the required input, the turbulent mean flow profile, can be determined.

7. CONCLUDING REMARKS

Silent owl flight has inspired a great deal of research seeking to reveal the secret of acoustic stealth. Technical approaches toward this goal have largely followed along one of two paths. First, from a comparative biology point of view, the foraging behavior and morphology of owls have been examined among owl species and non-owl species to determine the cause of silent flight. Second, from a physics-oriented point of view, the owl wing specializations are tacitly assumed to be the source of their silent flight, and the physical differences between owl wing features and standard airfoils are investigated to identify how they modify the known mechanisms of aerodynamic noise generation. These approaches are convergent but have not yet definitively determined how owls fly silently.

To close this gap in knowledge on the roles of owl wing specializations and other factors that may contribute to their aerodynamic noise suppression, researchers need owl flight noise data from moderate- and smaller-sized owls that also possess the specialized owl-wing attributes. A deeper connection of these attributes to the evolutionary pressures on different owl species requires a phylogenetic correlation of owl wing specializations with complete physical and noise measurements, where data and tools from the aeroacoustics and biology communities are necessary to make progress.

New mechanisms for aerodynamic noise mitigation based on owls stand to favorably impact the energy, aerospace, and transportation industries, where the biological constraints of the owl can be removed and the mechanical design can be optimized for noise suppression based on the flow physics. However, the principal obstacle to the design of owl-inspired technologies remains the lack of understanding of the essential physics of silent owl flight, even at the bird scale. Indeed, the design and testing of an artificial owl wing with modular wing features and a favorable comparison with actual bird wings would be a leap forward in demonstrating the essential physics and in leveraging that understanding to other applications in low-speed flows at different scales. This pursuit of new strategies for broadband noise suppression is likely to accompany and encourage advances in analytical modeling of noise generation, acoustical measurement techniques, and computational aeroacoustics.

SUMMARY POINTS

1. Many owls suppress noise within the audible range of their prey and of themselves, especially the noise generated at the wing trailing edge. Acoustic measurements of live owls show accelerated reductions in aerodynamic noise above 1.6 kHz, extending into the ultrasonic range.
2. The considerable variation in hunting behavior and wing structure across owl species suggests that particular physical noise generation mechanisms and sound sources are being suppressed. Attributes such the downy wing surface also appear on some non-owl species, and additional effort is required to determine the role of these wing specializations on aerodynamic noise generation and, possibly, if noise mitigation is present on these non-owl species.
3. The trailing-edge fringe and the downy wing surface have inspired a noise-reduction device that appears, at least so far in wind tunnel tests, to significantly reduce trailing-edge noise on a realistic wind turbine airfoil section. However, a detailed physical understanding of this process is still lacking.
4. There is good evidence that the leading-edge comb plays a role in noise reduction at high angles of attack, apparently by controlling otherwise noisy flow at the wing tip.

FUTURE ISSUES

1. Due to the numerous features believed to be the cause of silent owl flight, it is reasonable to expect that only a reduction to practice of noise-reduction strategies via, say, an owl-sized air vehicle that replicates the owl noise spectrum would prove that the features for silent owl flight had been identified. However, the physical basis for this reduction is desired, which can be used in applications beyond the parameter space spanned by owl flight.
2. Although the owl wing attributes reviewed here are likely responsible for the suppression of aerodynamic noise, these features alone may not be responsible for all of the noise reduction observed in owl flyover experiments. In this case, recent advances in the kinematic measurements of live birds may be pursued for clues about how owls manipulate body and wing motions to mask their aerodynamic noise.
3. Acoustical data for owl flight are limited to barn owls, but noise measurements of smaller owl species with different foraging behaviors are desired to examine the roles of attribute size on noise suppression. Furthermore, these data are needed to determine if smaller owl species are also able to achieve silent flight.
4. Is there an evolutionary basis for the wing attributes allegedly responsible for silent owl flight? To address this question, a phylogenetic comparative analysis is needed, which would require physical measurements of many owl and other bird species as well as complementary acoustic measurements to be able to draw firm conclusions from the biology side. This line of inquiry is an opportunity for cross-disciplinary investigations between fluid mechanists and biologists.

5. Geometrical modifications of wing edges and surfaces lead to changes in the local flow that can affect the noise generated. An improved physical understanding is sought of flow effects local to edge and surface geometries and their role in noise generation and propagation into the far field. Researchers will need to examine the robustness of such physics in applications and to construct models to inform the application of noise-reduction technology to devices at different speeds and scales than those of the owl.
6. Owl-inspired noise-reduction strategies may come at the cost of diminished aerodynamic performance, where the means to rapidly assess the intrinsic aerodynamic–aeroacoustic trade-off is likely to be an important consideration in industrial conceptual designs.

DISCLOSURE STATEMENT

The authors are not aware of any biases that might be perceived as affecting the objectivity of this review.

ACKNOWLEDGMENTS

The authors gratefully acknowledge the financial support of the National Science Foundation under grants 0965248 (IRFP), 1805692, and 1846852 (CAREER) (J.W.J.); the Office of Naval Research (ONR) under grant N00014-14-1-0242 (J.W.J.) and ONR Global grant N62909-12-1-7116 (N.P. and J.W.J.); and the Air Force Office of Scientific Research under grants FA9550-15-1-0148 and FA9550-19-1-0095 (J.W.J.). The authors thank Mr. Riley Saeger for collecting and providing his chord-length measurements of spread owl wings. Lastly, the authors acknowledge the inspiration and early support of the late Professor Geoffrey Lilley OBE, whose interest in silent owl flight gave impulse to much of the modern research into owl aeroacoustics.

LITERATURE CITED

Amiet RK. 1976. Noise due to turbulent flow past a trailing edge. *J. Sound Vib.* 47:387–93

Antonia RA, Luxton RE. 1972. The response of a turbulent boundary layer to a step change in surface roughness. Part 2. Rough-to-smooth. *J. Fluid Mech.* 53:737–57

Ayton LJ, Chaitanya P. 2017. Analytical and experimental investigation into the effects of leading-edge radius on gust–aerofoil interaction noise. *J. Fluid Mech.* 829:780–808

Ayton LJ, Peake N. 2016. Interaction of turbulence with the leading-edge stagnation point of a thin aerofoil. *J. Fluid Mech.* 798:436–56

Bachmann TW. 2010. *Anatomical, morphometrical and biomechanical studies of barn owls' and pigeons' wings*. PhD Thesis, RWTH Aachen University, Aachen, Ger.

Bachmann T, Blazek S, Erlinghagen T, Baumgartner W, Wagner H. 2012a. Barn owl flight. In *Nature-Inspired Fluid Mechanics*, ed. C Tropea, H Bleckmann, pp. 101–17. Berlin: Springer

Bachmann T, Klän S, Baumgartner W, Klaas M, Schröder W, Wagner H. 2007. Morphometric characterisation of wing feathers of the barn owl *Tyto alba pratincola* and the pigeon *Columba livia*. *Front. Zool.* 4:23

Bachmann T, Mühlenbruch G, Wagner H. 2011. The barn owl wing: An inspiration for silent flight in the aviation industry? In *Bioinspiration, Biomimetics, and Bioreplication*, ed. RJ Martin-Palma, A Lakhtakia, Pap. 7975 0N. Bellingham, WA: SPIE

Bachmann T, Wagner H. 2011. The three-dimensional shape of serrations at barn owl wings: towards a typical natural serration as a role model for biomimetic applications. *J. Anat.* 219:192–202

Bachmann T, Wagner H, Tropea C. 2012b. Inner vane fringes of barn owl feathers reconsidered: morphometric data and functional aspects. *J. Anat.* 221:1–8

Bodling A, Sharma A. 2019a. Numerical investigation of low-noise airfoils inspired by the down coat of owls. *Bioinspir. Biomimet.* 14:016013

Bodling A, Sharma A. 2019b. Numerical investigation of noise reduction mechanisms in a bio-inspired airfoil. *J. Sound Vib.* 453:314–27

Bostwick KS, Prum RO. 2003. High-speed video analysis of wing-snapping in two manakin clades (Pipridae: Aves). *J. Exp. Biol.* 206:3693–706

Brooks TF, Pope DS, Marcolini MA. 1989. *Airfoil self-noise and prediction*. NASA Tech. Rep. 1218, NASA, Washington, DC

Cannell PA. 1975. Edge scattering of aerodynamic sound by a lightly loaded elastic half-plane. *Proc. R. Soc. Lond. A* 347:213–38

Cannell PA. 1976. Acoustic edge scattering by a heavily loaded elastic half-plane. *Proc. R. Soc. Lond. A* 350:71–89

Cavalieri AVG, Wolf WR, Jaworski JW. 2016. Numerical solution of acoustic scattering by finite perforated elastic plates. *Proc. R. Soc. A* 472:20150767

Chaitanya P, Joseph P, Narayanan S, Vanderwel C, Turner J, et al. 2017. Performance and mechanism of sinusoidal leading edge serrations for the reduction of turbulence–aerofoil interaction noise. *J. Fluid Mech.* 818:435–64

Chavarin A, Luhar M. 2019. Resolvent analysis for turbulent channel flow with riblets. *AIAA J.* In press

Choi H, Moin P, Kim J. 1993. Direct numerical simulation of turbulent flow over riblets. *J. Fluid Mech.* 255:503–39

CAA (Civil Aviat. Auth.). 2018. *Departure noise mitigation: main report*. Tech. Rep. 1691, Civil Aviat. Auth., West Sussex, UK

Clark CJ. 2016. Locomotion-induced sounds and sonations: mechanisms, communication function, and relationship with behavior. In *Vertebrate Sound Production and Acoustic Communication*, ed. R Suthers, W Fitch, R Fay, A Popper, pp. 83–117. Cham, Switz.: Springer

Clark CJ, Prum RO. 2015. Aeroelastic flutter of feathers, flight and the evolution of non-vocal communication in birds. *J. Exp. Biol.* 218:3520–27

Clark IA. 2017. *Bio-inspired control of roughness and trailing edge noise*. PhD Thesis, Virginia Polytech. Inst. State Univ., Blacksburg, VA

Clark IA, Alexander WN, Devenport W, Glegg S, Jaworski JW, et al. 2015. *Bio-inspired trailing edge noise control*. Paper presented at AIAA/CEAS Aeroacoustics Conference, 21st, Dallas, TX, AIAA Pap. 2015-2365

Clark IA, Alexander WN, Devenport W, Glegg S, Jaworski JW, et al. 2017. Bioinspired trailing-edge noise control. *AIAA J.* 55:740–54

Clark IA, Daly CA, Devenport W, Alexander WN, Peake N, et al. 2016. Bio-inspired canopies for the reduction of roughness noise. *J. Sound Vib.* 385:33–54

Crighton DG. 1975. Basic principles of aerodynamic noise generation. *Prog. Aerosp. Sci.* 16:31–96

Crighton DG. 1991. Airframe noise. In *Aeroacoustics of Flight Vehicles: Theory and Practice*, Vol. 1, *Noise Sources*, ed. HH Hubbard, pp. 391–447. Hampton, VA: NASA Langley Res. Cent.

Crighton DG, Leppington FG. 1970. Scattering of aerodynamic noise by a semi-infinite compliant plate. *J. Fluid Mech.* 43:721–36

Curle N. 1955. The influence of solid boundaries upon aerodynamic sound. *Proc. R. Soc. Lond. A* 231:505–14

Dowell EH, ed. 2015. *A Modern Course in Aeroelasticity*. Dordrecht, Neth.: Kluwer Acad. 5th ed.

Dubois AD. 1924. A nuptial song-flight of the short-eared owl. *Auk* 41:260–63

Dyson ML, Klump GM, Gauger B. 1998. Absolute hearing thresholds and critical masking ratios in the European barn owl: a comparison with other owls. *J. Comp. Physiol. A* 182:695–702

FAA (Fed. Aviat. Admin.). 2019. *Continuous lower energy, emissions, and noise (CLEEN) program*, accessed Feb. 19. **https://www.faa.gov/about/office_org/headquarters_offices/apl/research/aircraft_technology/cleen/**

Ffowcs Williams JE. 1972. The acoustics of turbulence near sound-absorbent liners. *J. Fluid Mech.* 51:737–49

Ffowcs Williams JE. 1977. Aeroacoustics. *Annu. Rev. Fluid Mech.* 9:447–68

A landmark experimental study of airfoil trailing-edge noise across a very broad parameter range.

A key numerical investigation of the effects of porosity and elasticity on noise from finite-chord airfoils.

Wind tunnel demonstration of an owl-inspired trailing-edge noise control device.

Ffowcs Williams JE, Hall LE. 1970. Aerodynamic sound generation by turbulent flow in the vicinity of a scattering half plane. *J. Fluid Mech.* 40:657–60

The first paper to identify the famous fifth-power Mach number dependence of trailing-edge noise.

Finez A, Jondeau E, Roger M, Jacob MC. 2010. *Broadband noise reduction with trailing edge brushes*. Paper presented at AIAA/CEAS Aeroacoustics Conference, 13th, Stockholm, AIAA Pap. 2010-3980

Fink MR, Bailey DA. 1980. *Airframe noise reduction studies and clean-airframe noise investigation*. NASA Contract. Rep. 159311, NASA, Washington, DC

Finnigan J. 2000. Turbulence in plant canopies. *Annu. Rev. Fluid Mech.* 32:519–71

Fournier JP, Dawson JW, Mikhail A, Yack JE. 2013. If a bird flies in the forest, does an insect hear it? *Biol. Lett.* 9:20130319

George AR, Najjar FE, Kim YN. 1980. *Noise due to tip vortex formation on lifting rotors.* Paper presented at Aeroacoustics Conference, 6th, Hartford, CT, AIAA Pap. 1980-1010

A detailed experimental study, including acoustic source location, using prepared owl wings to demonstrate the possible role of the leading-edge comb in silent flight at high angles of attack.

Geyer TF, Claus VT, Hall PM, Sarradj E. 2017. Silent owl flight: the effect of the leading edge comb. *Int. J. Aeroacoustics* 16:115–34

Geyer TF, Sarradj E. 2014. *Trailing edge noise of partially porous airfoils*. Paper presented at AIAA/CEAS Aeroacoustics Conference, 20th, Atlanta, GA, AIAA Pap. 2014-3039

Geyer TF, Sarradj E, Fritzsche C. 2009. Silent owl flight: experiments in the aeroacoustic wind tunnel. In *NAG/DAGA International Conference on Acoustics*, ed. MM Boone, pp. 734–36. Red Hook, NY: Curran

Geyer TF, Sarradj E, Fritzsche C. 2010. Measurement of the noise generation at the trailing edge of porous airfoils. *Exp. Fluids* 48:291–308

Geyer TF, Sarradj E, Fritzsche C. 2013. Silent owl flight: comparative acoustic wind tunnel measurements on prepared wings. *Acta Acust. United Acust.* 99:139–53

Graham RR. 1934. The silent flight of owls. *J. R. Aeronaut. Soc.* 38:837–43

Gruschka HD, Borchers IU, Coble JG. 1971. Aerodynamic noise produced by a gliding owl. *Nature* 233:409–11

Hajian R, Jaworski JW. 2017. The steady aerodynamics of aerofoils with porosity gradients. *Proc. R. Soc. A* 473:20170266

Hajian R, Jaworski JW. 2019. Noncirculatory fluid forces on panels with porosity gradients. *AIAA J.* 57:870–75

Hayden RE. 1976. *Reduction of noise from airfoils and propulsive lift systems using variable impedance systems*. Paper presented at AIAA Aeroacoustics Conference, 3rd, Palo Alto, CA, AIAA Pap. 1976-500

Hayden RE, Kadman Y, Chanaud RC. 1972. *A study of the variable impedance surface concept as a means for reducing noise from jet interaction with deployed lift-augmenting flaps*. NASA Tech. Rep. CR-112166, NASA, Washington, DC

Heffner H, Masterton B. 1980. Hearing in Glires: domestic rabbit, cotton rat, feral house mouse, and kangaroo rat. *J. Acoust. Soc. Am.* 68:1584–99

Herr M. 2007. *Design criteria for low-noise trailing-edges*. Paper presented at AIAA/CEAS Aeroacoustics Conference, 13th, Rome, Italy, AIAA Pap. 2007-3470

Herr M, Dobrzynski W. 2005. Experimental investigations in low-noise trailing-edge design. *AIAA J.* 43:1167–75

Herr M, Reichenberger J. 2011. *In search of airworthy trailing-edge noise reduction means*. Paper presented at AIAA/CEAS Aeroacoustics Conference, 17th, Portland, Oregon, AIAA Pap. 2011-2780

Hersh AS, Sodermant PT, Hayden RE. 1974. Investigation of acoustic effects of leading-edge serrations on airfoils. *J. Aircr.* 11:197–202

Hertel H. 1963. *Struktur, Form, Bewegung*. Mainz, Ger.: Krausskopf-Verlag

High Level Group Aviat. Res. 2011. *Flightpath 2050: Europe's vision for aviation*. Tech. Rep., ACARE (Advis. Counc. Aeronaut. Res. Eur.), Brussels, Belg. **https://ec.europa.eu/transport/sites/transport/files/modes/air/doc/flightpath2050.pdf**

Hileman J, Spakovszky Z, Drela M, Sargeant M. 2007. *Airframe design for "silent aircraft."* Paper presented at AIAA Aerospace Sciences Meeting, 45th, Reno, NV, AIAA Pap. 2007-453

Howe MS. 1978. A review of the theory of trailing edge noise. *J. Sound Vib.* 61:437–65

Howe MS. 1979. On the added mass of a perforated shell, with application to the generation of aerodynamic sound by a perforated trailing edge. *Proc. R. Soc. Lond. A* 365:209–33

Howe MS. 1992. Sound produced by an aerodynamic source adjacent to a partly coated, finite elastic plate. *Proc. R. Soc. Lond. A* 436:351–72

Howe MS. 1993. Structural and acoustic noise produced by turbulent flow over an elastic trailing edge. *Proc. R. Soc. Lond. A* 442:533–54

Howe MS. 2003. *Theory of Vortex Sound*. Cambridge, UK: Cambridge Univ. Press

Intaratep N, Alexander WN, Devenport WJ, Grace SM, Dropkin A. 2016. *Experimental study of quadcopter acoustics and performance at static thrust conditions*. Paper presented at AIAA/CEAS Aeroacoustics Conference, 22nd, Lyon, France, AIAA Pap. 2016-2873

Iosilevskii G. 2011. Aerodynamics of permeable membrane wings. *Eur. J. Mech. B* 30:534–42

Iosilevskii G. 2013. Aerodynamics of permeable membrane wings. Part 2: seepage drag. *Eur. J. Mech. B* 39:32–41

Jaworski JW, Peake N. 2013. Aerodynamic noise from a poroelastic edge with implications for the silent flight of owls. *J. Fluid Mech.* 723:456–79

Johnsgard PA. 2002. *North American Owls: Biology and Natural History*. Washington, DC: Smithsonian Inst. 2nd ed.

Khorrami MR, Choudhari MM. 2003. *Application of passive porous treatment for slat trailing edge noise*. NASA Tech. Rep. TM-2003-212416, NASA Langley Res. Cent., Hampton, VA

Kisil A, Ayton LJ. 2018. Aerodynamic noise from rigid trailing edges with finite porous extensions. *J. Fluid Mech.* 836:117–44

Klän S, Bachmann T, Klaas M, Wagner H, Schröder W. 2009. Experimental analysis of the flow field over a novel owl based airfoil. *Exp. Fluids* 46:975–89

Klän S, Burgmann S, Bachmann T, Klaas M, Wagner H, Schröder W. 2012. Surface structure and dimensional effects on the aerodynamics of an owl-based wing model. *Eur. J. Mech. B* 33:58–73

Konishi M. 1973. How the owl tracks its prey. *Am. Sci.* 61:414–24

Kornecki A, Dowell EH, O'Brien J. 1976. On the aeroelastic instability of two-dimensional panels in uniform incompressible flow. *J. Sound Vib.* 47:163–78

Kroeger RA, Gruschka HD, Helvey TC. 1972. *Low speed aerodynamics for ultra-quiet flight*. Tech. Rep. AFFDL-TR-71-75, Air Force Flight Dyn. Lab., Wright-Patterson Air Force Base, Ohio

Lighthill MJ. 1952. On sound generated aerodynamically. I. General theory. *Proc. R. Soc. Lond. A* 211:564–87

Lighthill MJ. 1954. On sound generated aerodynamically. II. Turbulence as a source of sound. *Proc. R. Soc. Lond. A* 222. **https://doi.org/10.1098/rspa.1954.0049**

Lilley GM. 1998. *A study of the silent flight of the owl*. Paper presented at AIAA/CEAS Aeroacoustics Conference, 4th, Toulouse, France, AIAA Pap. 1998-2340

Lyu B, Ayton LJ, Chaitanya P. 2019. On the acoustic optimality of leading-edge serration profiles. *J. Sound Vib.* In press

Lyu B, Azarpeyvand M. 2017. On the noise prediction for serrated leading edges. *J. Fluid Mech.* 826:205–34

Lyu B, Azarpeyvand M, Sinayoko S. 2016. Prediction of noise from serrated trailing edges. *J. Fluid Mech.* 793:556–88

Millican AJ, Clark I, Devenport W, Alexander WN. 2017. *Owl-inspired trailing edge noise treatments: acoustic and flow measurements*. Paper presented at AIAA Aerospace Sciences Meeting, 35th, Grapevine, TX, AIAA Pap. 2017-1177

Myers MR, Kerschen EJ. 1995. Influence of incidence angle on sound generation by airfoils interacting with high-frequency gusts. *J. Fluid Mech.* 292:271–304

Neuhaus W, Bretting H, Schweizer B. 1973. Morphologische und funktionelle Untersuchungen über den "lautlosen" Flug der Eulen (*Strix aluco*) im Vergleich zum Flug der Enten (*Anas platyrhynchos*). *Biol. Zentral.* 92:495–512

Norberg RÅ. 1970. Hunting technique of Tengmalm's owl *Aegolius funereus* (L.). *Ornis Scand.* 1:51–64

Oerlemans S, Sijtsma P, Méndez López B. 2007. Location and quantification of noise sources on a wind turbine. *J. Sound Vib.* 299:869–83

Payne RS. 1962. How the barn owl locates its prey by hearing. *Living Bird* 1:151–59

Modeling of the effects of poroelasticity on trailing-edge noise in the context of silent owl flight.

Comprehensive early investigation and analysis of the mechanisms involved in the silent flight of live owls.

The seminal paper on the theory of noise generation by aerodynamic flow.

A thorough discussion of noise sources on wind turbines, a possible application area for owl-inspired noise technology.

Payne RS. 1971. Acoustic location of prey by barn owls (*Tyto alba*). *J. Exp. Biol.* 54:535–73

Pimenta C, Wolf WR, Cavalieri AVG. 2018. A fast numerical framework to compute acoustic scattering by poroelastic plates of arbitrary geometry. *J. Comput. Phys.* 373:763–83

Rao C, Ikeda T, Nakata T, Liu H. 2017. Owl-inspired leading-edge serrations play a crucial role in aerodynamic force production and sound suppression. *Bioinspir. Biomimet.* 12:046008

Roulin A, Mangels J, Wakamatsu K, Bachmann T. 2013. Sexually dimorphic melanin-based colour polymorphism, feather melanin content, and wing feather structure in the barn owl (*Tyto alba*). *Biol. J. Linn. Soc.* 109:562–73

Important comparative measurements of owl noise in flight against other birds using an acoustic array.

Sarradj E, Fritzsche C, Geyer T. 2011. Silent owl flight: flyover noise measurements. *AIAA J.* 49:769–79

Seeley BA. 2015. *Regional sky transit*. Paper presented at AIAA Aviation Technology, Integration, and Operations Conference, 15th, Dallas, TX, AIAA Pap. 2015-3184

Sharma AS, McKeon BJ. 2013. On coherent structure in wall turbulence. *J. Fluid Mech.* 728:196–238

Sick H. 1937. Morphologisch-funktionelle Untersuchungen über die Feinstruktur der Vogelfeder. *J. Ornithol.* 85:206–372

Smits AJ, Wood DH. 1985. The response of turbulent boundary layers to sudden perturbations. *Annu. Rev. Fluid Mech.* 17:321–58

Thorpe WH, Griffin DR. 1962a. Lack of ultrasonic components in the flight noise of owls. *Nature* 193:594–95

The earliest reported experimental observations of aerodynamic noise suppression by owls in flight.

Thorpe WH, Griffin DR. 1962b. The lack of ultrasonic components in the flight noise of owls compared with other birds. *Ibis* 104:256–57

Turner JM, Kim JW. 2017. Aeroacoustic source mechanisms of a wavy leading edge undergoing vortical disturbances. *J. Fluid Mech.* 811:582–611

Wagner H, Weger M, Klaas M, Schröder W. 2017. Features of owl wings that promote silent flight. *Interface Focus* 7:20160078

Walsh MJ. 1983. Riblets as a viscous drag reduction technique. *AIAA J.* 21:485–86

Wang M, Freund JB, Lele SK. 2006. Computational prediction of flow-generated sound. *Annu. Rev. Fluid Mech.* 38:483–512

Weger M, Wagner H. 2016. Morphological variations of leading-edge serrations in owls (*Strigiformes*). *PLOS ONE* 11:e0149236

Weger M, Wagner H. 2017. Distribution of the characteristics of barbs and barbules on barn owl wing feathers. *J. Anat.* 230:734–42

Wink M, El-Sayed AA, Sauer-Gürth H, Gonzalez J. 2009. Molecular phylogeny of owls (*Strigiformes*) inferred from DNA sequences of the mitochondrial cytochrome b and the nuclear RAG-1 gene. *Ardea* 97:581–91

Winzen A, Klaas M, Schröder W. 2013. High-speed PIV measurements of the near-wall flow field over hairy surfaces. *Exp. Fluids* 54:1472

Wolf T, Konrath R. 2015. Avian wing geometry and kinematics of a free-flying barn owl in flapping flight. *Exp. Fluids* 56:28

Zhou BY, Koh SR, Gauger NR, Meinke M, Schröder W. 2018. A discrete adjoint framework for trailing-edge noise minimization via porous material. *Comput. Fluids* 172:97–108

Annual Review of
Fluid Mechanics

Volume 52, 2020

Contents

Indexes

Errata

An online log of corrections to *Annual Review of Fluid Mechanics* articles may be found at http://www.annualreviews.org/errata/fluid